Volume 1 | Number 1 | Jan 2013 | Pages 1–100

Green Chemistry

Cutting-edge research for a greener sustainable future

www.rsc.org/greenchem

Stille couplings in water @RT

ROYAL SOCIETY OF CHEMISTRY

ROYAL SOCIETY OF CHEMISTRY

www.rsc.org/greenchem

Graphical Abstract

By application of reasonably low gas pressure, formation of metallic aluminum is completely suppressed during the solid-state mechanochemical synthesis of AlH_3 at room temperature.

Journal Name

ARTICLE

Solvent-free Mechanochemical Synthesis of Alane, AlH$_3$: Effect of Pressure on the Reaction Pathway

S. Gupta,[a,*] T. Kobayashi,[a] I.Z. Hlova,[a,b] J.F. Goldston,[a,c] M. Pruski,[a,c,*] and V.K. Pecharsky[a,b,*]

Nearly quantitative mechanochemical synthesis of non-solvated AlH$_3$ from lithium aluminium hydride (LiAlH$_4$) and aluminium chloride (AlCl$_3$) has been achieved at room temperature under reasonably low pressure of hydrogen (210 bar) or inert gas (125 bar for He or 90 bar for Ar). X-ray diffraction, solid-state ^{27}Al NMR spectroscopy, and temperature programmed desorption analysis of as-milled materials reveal a nearly complete conversion of a 3:1 (molar) mixture of LiAlH$_4$ and AlCl$_3$ to a 4:3 (molar) mixture of AlH$_3$ and LiCl in ca. 30 min. By applying pressure of 210 bar or less (depending on the gas: hydrogen, helium, or argon), competing reactions leading to formation of metallic aluminium can be completely suppressed. X-ray diffraction and NMR analyses of products extracted at various stages of the mechanochemical reaction between LiAlH$_4$ and AlCl$_3$ reveal, for the first time, that the solid-state transformation proceeds with LiAlCl$_4$ as an intermediate. Evidently, the critical pressure required to suppress the formation of metallic aluminium depends on the rate at which mechanical energy is supplied during milling. For example, the critical pressure is reduced from 210 bar to 1 bar of hydrogen when the milling speed of a standard planetary mill is reduced from 300 rpm to 150 rpm, although at the expense of sluggish kinetics and much longer reaction time.

Introduction

Realization of declining natural reserves of easily accessible carbon-based energy sources, and the deleterious environmental impact of their indiscriminate use to meet skyrocketing energy demands have led to sustained efforts to transition to environmentally benign and sustainable energy sources.[1] Hydrogen is considered an ideal energy carrier as it has large gravimetric energy density (~142 MJ kg^{-1}), is abundant in the form of H$_2$O, and produces no harmful emissions when utilized in PEM fuel cells and other energy conversion devices.[1–4] Besides its high energy value and clean oxidation, hydrogen may be sustainably produced by electrolysis of water using zero-carbon wind, off-peak hydroelectric and solar power, among other practical methods.[5]

In order to enable distributed fuel-cell technologies based on chemically stored hydrogen, materials exceeding 8–10 wt.% hydrogen capacity, and capable of releasing hydrogen at a high rate below 100 °C are required.[6] Such stringent restraints severely limit the choice of materials currently available for practical hydrogen storage. In this regard, AlH$_3$ (aluminum trihydride or alane) is extremely promising since it combines high gravimetric and volumetric hydrogen capacities of 10.1 wt % and 149 kg m^{-3}, respectively, and delivers uncontaminated H$_2$ in a single step around 100 °C or less depending upon the method of preparation.[7] Despite these impressive figures, strong sensitivity of AlH$_3$ to oxidation and

hydrolysis, and its flammability are challenging safety issues that need to be addressed during storage and use in transportation applications. Suitable and safe methods for use of AlH$_3$ as a fuel, such as formulation as a slurry, have been suggested.[8] Moreover, AlH$_3$ is kinetically metastable at room temperature and releases hydrogen in an endothermic process, which provides inherent stability to the system by self-limiting the hydrogen release reaction.[9] The enormous potential offered by AlH$_3$ is, however, much reduced by the lack of a simple and direct method for its synthesis in a pure form, given its thermodynamic instability ($\Delta G°_f \approx$ 46 kJ mol^{-1}).[10] The most preferred route to synthesize AlH$_3$ would be to directly combine elemental Al and gaseous hydrogen according to Eq. 1:

$$Al + 3/2\ H_2 \rightarrow AlH_3 \qquad (1)$$

However, according to the p,T state diagram of AlH$_3$, direct hydrogenation of elemental Al by gaseous H$_2$ is possible only at pressures exceeding 2.5 GPa (25,000 bar) and temperature close to 300 °C, or 0.7 GPa (7,000 bar) at room temperature, which is impractical on an industrial scale.[11] Alternatively, AlH$_3$ can be obtained under much milder conditions by the reaction of LiAlH$_4$ and AlCl$_3$ in diethyl ether (Et$_2$O), commonly known as the Schlesinger reaction:[12]

$$3LiAlH_4 + AlCl_3 + nEt_2O \rightarrow 4AlH_3 \cdot nEt_2O + 3LiCl \qquad (2)$$

The reaction, first reported in 1947, leads to an ether adduct of AlH_3; however, removal of ether by heating usually leads to decomposition of a significant fraction of the prepared alane. Subsequently, several methods of producing non-solvated AlH_3 from its ether adduct were proposed with limited success and reproducibility.[13] As described in US patents by the Dow Chemical Co. (1974) and by Bower *et al.* (1976), AlH_3 can be obtained in a non-solvated form by desolvation of the AlH_3-ether adduct in the presence of excess $LiAlH_4$ and $LiBH_4$ that help reduce the temperature of desolvation, and hence minimize the decomposition of AlH_3.[14] However, this method of production of AlH_3 is quite sensitive to heating conditions, and often lacks good reproducibility. Thus, a method of performing this conversion in a solvent-free environment for a direct yield of non-solvated AlH_3 is highly desirable. A recent report demonstrated that a low-temperature (75 °C), thermochemical transformation in the solid state is feasible due to the favorable change in the Gibbs free energy:[15]

$$3LiAlH_4 + AlCl_3 \rightarrow 4AlH_3 + 3LiCl \quad \Delta_rG_{298K} = -191 \text{ kJ mol}^{-1}, \Delta_rG_{77K} = -158 \text{ kJ mol}^{-1} (3)$$

To carry out this thermochemical transformation at a reasonable conversion rate, however, necessitates pre-mixing of reactants, preferably in a ball mill, followed by compaction or continuous mixing during the heat treatment. Also, in a thermal reaction, one may encounter problems with local overheating, formation of low melting eutectics, and very rapid, nearly explosive decomposition to metallic Al and hydrogen.[16]

Apart from the aforementioned methods of synthesis of AlH_3, more convenient, one-step solvent-free mechanochemical syntheses have also been investigated to accomplish the transformation shown in Eq. 3.[17,18] For example, synthesis of AlD_3 was accomplished by ball-milling $LiAlD_4$ and $AlCl_3$ taken in 3:1 molar ratio in a planetary mill, both at room temperature and at −196 °C.[17] Milling at room temperature results in a mixture of α and α'-AlD_3 and LiCl along with metallic Al. Brinks *et al.* suggested that large temperature spike(s) during mechanochemical processing may have caused the decomposition of AlH_3 (about 60 % of the stoichiometric amount) to metallic Al. As indicated by the free energy change for Eq. 3, the solid-state reaction is also feasible at −196 °C, and this was successfully employed by Brinks *et al.* to suppress the formation of metallic Al.[17] Although the mechanochemical reaction to synthesize AlH_3 at −196 °C significantly reduces the formation of metallic Al, cooling of the system to cryogenic temperatures may pose procedural and technical challenges that could be detrimental to large-scale production of AlH_3 using this method.

As search for efficient and cost-effective methods to synthesize metal hydrides continues, mechanochemical synthesis in the presence of reactive gases has been the method of choice for selected classes of hydrides.[4,19] This entails mechanochemical processing of solids under reactive gases such as hydrogen, diborane and other, to form hydrides.[20,21] Apart from serving as one of the reactants, the high pressure gaseous environment may also affect the milling intensity thereby influencing the reaction pathway.

Recently, we developed capability to carry out mechanochemical reactions under gas pressure as high as 350 bar and reported solid-state synthesis of AlH_3 from LiH and $AlCl_3$.[22] However, stoichiometric (3:1 molar LiH:$AlCl_3$) reaction carried out under our highest working pressure of hydrogen yields mostly metallic Al. Nearly quantitative yield of AlH_3 has been achieved when mechanochemical processing was carried out in three steps starting from a LiH-rich composition gradually adjusting it to match the ideal 3:1 LiH:$AlCl_3$ stoichiometry.[22] Such multistep process is relatively complex, and simpler synthetic routes are highly desirable. In this work we describe a simple, efficient, one-step synthesis of AlH_3 that

leads, for the first time, to a complete suppression of the parasitic formation of metallic Al during room-temperature execution of the solid-state mechanochemical reaction between $LiAlH_4$ and $AlCl_3$. We also uncover the mechanistic pathway of this mechanochemical solid-state reaction, and elucidate the effect of gas pressure and milling intensity. Heretofore unreported, control of this reaction pathway by the application of gas pressure may open new avenues for facile mechanochemical synthesis of otherwise metastable advanced functional materials.

Experimental Section

Materials and mechanochemical processing. Starting materials – $LiAlH_4$ (Aldrich, 98 %), and $AlCl_3$ (Aldrich, 99.99 %) – were used as-received. All manipulations, including sample loading and extraction, were carried out in an argon-filled glove box with the oxygen and moisture levels controlled at less than 5 ppm (v/v). In a typical mechanochemical reaction for synthesis of AlH_3, an approximately 1 g mixture of $LiAlH_4$ and $AlCl_3$ in the molar ratio of 3:1 was weighed and transferred to custom-built high-pressure milling containers. The containers with an internal volume of 5.62 in^3 (~92 ml) have been fabricated from 316L grade stainless steel and lined with 440C hardened stainless steel in order to minimize wear and related sample contamination during milling. Twenty chrome steel balls (AISI E52100, ρ~7.83 g cm^{-3}) weighing 8.3 g each were added to the containers, which were then sealed under argon. The containers were then evacuated and filled with either zero-grade H_2 (Linweld, 99.999%) or He (Matheson, 99.999%) or high-purity Ar (99.996 %) to the desired pressure ranging between 1 and 250 bar. A two-station horizontal planetary mill (Fritsch, Pulverisette 7) was employed for milling. As the *standard condition*, milling was carried out at 300 rpm with ball-to-powder mass ratio (b:p) of ~160:1. The milling sequence alternated between forward and reverse directions for 2 min each with an intermittent pause of 1 min to keep the average temperature in the vial as close to room temperature as possible. Unless otherwise noted, this milling condition was used throughout this study. The samples are denoted to indicate the gas pressure, gas type and milling time. For example, a 3:1 molar mixture of $LiAlH_4$ and $AlCl_3$ milled under 250 bar of hydrogen pressure (p_{H_2}) for 60 min is referred to as *250H₂-60m*. Considering the high b:p ratio employed, potential contamination with the milling media (steel) was verified by measuring magnetic properties of the product obtained after milling for 60 min. The absence of a ferromagnetic signal down to 2 K indicates that there were no detectable wear of the media and, therefore, no contamination of the samples. Also, to elucidate the mechanistic pathway, several experiments were performed in a SPEX 8000M mixer mill using a stainless steel container and milling media. Here, milling was carried out under argon atmosphere ($p_{Ar} = 1$ bar) for 60 min with a b:p of ~20:1. It may be noted that the SPEX mill affords relatively high-energy milling, and the containers utilized in this process were not pressurized.

X-ray powder diffraction analysis. The obtained products were characterized by powder X-ray diffraction (PXRD) analysis at room temperature on a PANalytical X'PERT diffractometer using Cu-$K_{\alpha1}$ radiation with a 0.02° 2θ step, in the 2θ range from 10° to 80°. During the measurements, a polyimide (Kapton) film was used to protect the samples from moisture and oxygen, which resulted in an amorphous-like background in the PXRD patterns in the range 13° ≤ 2θ ≤ 20°.

Solid-state NMR spectroscopy. The ^{27}Al solid-state (SS)NMR experiments were performed at 14.1 T on a Varian VNMRS 600 spectrometer and at 9.4 T on a Chemagnetics Infinity 400 spectrometer. Both instruments were equipped with 3.2-mm magic

angle spinning (MAS) probes operated at a MAS rate of 16 kHz. The samples were packed in MAS zirconia rotors in a glove box under argon atmosphere and were tightly capped to minimize the possibility of oxygen and moisture contamination. The one-dimensional ^{27}Al spectra were acquired using direct polarization with a single pulse (DP)MAS or via ^{1}H→^{27}Al cross-polarization (^{27}Al{^{1}H} CPMAS). For quantitative accuracy, the DPMAS spectra were acquired using a small flip angle of ~10°.[23,24] The CPMAS spectra represent ^{27}Al nuclei in dipolar contact with the protons located one to two bond distances away. High-power heteronuclear ^{1}H decoupling was achieved using the two-pulse phase-modulation (TPPM) method.[25] To provide high-resolution ^{27}Al spectra of selected samples, two-dimensional triple-quantum (3Q)MAS spectra were measured using the standard Z-filter method.[26,27] Detailed experimental conditions are given in the figure captions using the following symbols: B_0 is the static magnetic field, ν_{RF}^X is the radio frequency (RF) magnetic field applied to X nuclei, τ_{CP} is the cross-polarization time, Δt_1 is the increment of t_1 during two-dimensional acquisition, and τ_{RD} is the recycle delay. The ^{27}Al shifts were referenced to 1.0-M aqueous solutions of Al(NO$_3$)$_3$ at 0 ppm.

Temperature Programmed Desorption (TPD). For thermal desorption experiments, ca. 200 mg of as-prepared powder samples were loaded in a custom-built autoclave designed to work with an automatic volumetric Sievert's type gas sorption analyzer (PCTPro-2000 by Setaram) coupled to a residual gas analyzer (RGA100). This was followed by volume calibration of the free sample space, which consisted of three helium absorption-desorption cycles over a period of 30–40 min. In a typical desorption experiment, samples were heated at the rate of 4 °C/min up to 200 °C and soaked at that temperature until saturation was achieved.

Results and discussion

Mechanochemical synthesis. A 3:1 molar mixture of LiAlH$_4$ and AlCl$_3$ was initially milled for 30 min at two different hydrogen pressures, p_{H_2}=100 and 250 bar. The PXRD pattern of a dark-grey product 100H$_2$-30m (Fig. 1a, pattern a) shows mainly LiCl and metallic aluminum, along with small amounts of α'-AlH$_3$ and α-AlH$_3$ (Bragg peaks are designated in Fig.1a by '+' and '*', respectively), confirming the results reported by Brinks et al.[17] In contrast, a light-grey product 250H$_2$-30m (pattern d) consisted of only LiCl and α-AlH$_3$, with no metallic Al observed. The small amount of starting LiAlH$_4$ present in the latter sample indicates that the overall reaction given by Eq. 3 nears completion in 30 min, but is not finished. However, the reaction is complete after 60 min of milling, as only α-AlH$_3$ and LiCl could be observed in the corresponding PXRD pattern e. The differences in the composition of products of the above two reactions clearly suggest that a critical pressure (p_c) may exist, above which, the formation of metallic Al is completely suppressed at room temperature. Further, it is also clear from these results that the reaction is slower above p_c. It is also noted that only α-AlH$_3$ is obtained in the crystalline state upon completion of the reaction at p_{H_2}=250 bar, as confirmed by the observed diffraction peaks at 2θ~ 27.6, 38.4 and 40.5° representing the three strongest Bragg peaks corresponding to its rhombohedral structure (space group R-3c).[28]

The temperature-programmed hydrogen desorption of the sample 250H$_2$-60m (Fig.1(b)) leads to ~4.8 wt % H$_2$, which, considering the 98% purity of the starting LiAlH$_4$, corresponds to a quantitative yield of AlH$_3$ according to Eq. 3 (theoretical capacity of 4AlH$_3$+3LiCl is 4.85 wt.% H$_2$). In accordance with the reported thermal behavior of pure AlH$_3$,[29–31] hydrogen desorption occurs in a single-step process with the onset temperature close to 100 °C. Also,

in agreement with the observed presence of α'-AlH$_3$ and α-AlH$_3$ phases mixed with metallic Al in the sample prepared below p_c, a total of ~1.9 wt % H$_2$ evolves (Fig.1(b)) during the desorption of sample 100H$_2$-30m. Based on the amount of evolved hydrogen, only ~40% of available aluminum in the 100H$_2$-30m sample is in the form of AlH$_3$, while the remaining 60% has been converted to metallic Al during milling, in quantitative agreement with the results published by Brinks et al.[17] In both samples studied here, mass-spectroscopic analysis of desorbed gases indicates >99.7 % H$_2$, the rest being traces of air. The observed decrease in the desorption temperature in sample 100H$_2$-30m compared to 250H$_2$-60m results from the much-improved thermal conductivity facilitated by metallic Al finely dispersed throughout the sample, considering the 4 °C/min temperature ramping rate.
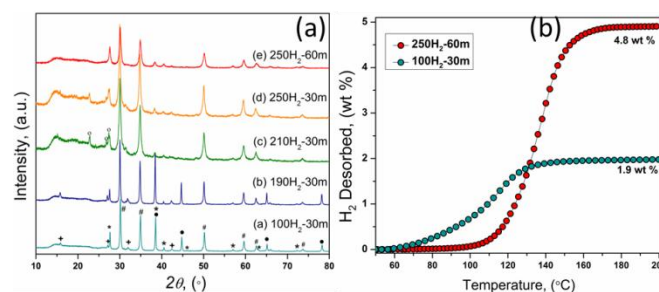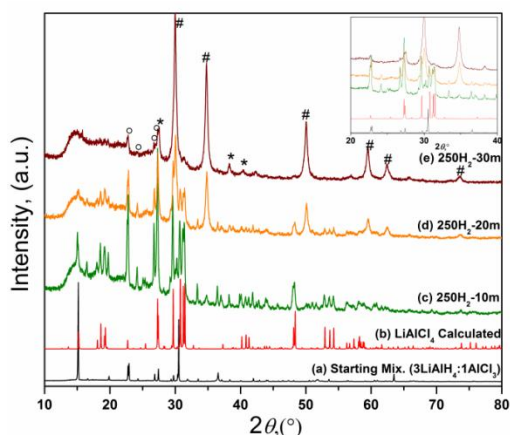

Figure 1. (a) X-ray diffraction patterns of the products obtained after mechanochemical processing of 3LiAlH$_4$+1AlCl$_3$ up to 60 min at H$_2$ pressures between 100 and 250 bar are shown. (*) α-AlH$_3$, (+) α'-AlH$_3$, (#) LiCl, (●) metallic aluminum, and (°) LiAlH$_4$. (b) Desorption curves obtained during heating of as-prepared samples between room temperature and 200 °C with ramping rate of 4 °C/min.

Determination of p_c. To estimate the value of p_c, several reactions were carried out at 100 bar ≤ p_{H_2} ≤ 250 bar under $standard$ $milling$ $conditions$. It is clear from the PXRD patterns that mixtures milled at p_{H_2} ≤ 190 bar (Fig. 1(a), patterns a and b) contain metallic Al, whereas mixtures milled under p_{H_2} ≥ 210 bar do not, establishing that the $p_c^{H_2}$ falls somewhere within the narrow range of 190 and 210 bar hydrogen. Finally, the orthorhombic α'-AlH$_3$ (Bragg peaks marked as '+') is a significant fraction of the product in reactions carried out below p_c, but not so much when p > p_c. Formation of a mixture of different polymorphs of AlH$_3$, and their subsequent conversion to the relatively more stable α-AlH$_3$ during this mechanochemical reaction have also been noted in earlier studies.[17,18]

Identification of intermediates. The progress of reaction 3 above the critical pressure has been studied by analyzing samples after different milling times at 250 bar. Figure 2 shows the PXRD patterns of products obtained after 10, 20 and 30 min of processing (samples 250H$_2$-10/20/30m, respectively) along with the reference pattern of a pristine 3:1 mixture of LiAlH$_4$ and AlCl$_3$. The diffraction patterns reveal that the starting LiAlH$_4$ remains in significant amount, while nearly all of the AlCl$_3$ has been consumed in 10 min as evidenced by significant reduction in the intensities of (001) and (002) reflections at 2θ ~15.1° and 30.4°, respectively. A new set of Bragg peaks appears, mainly between 2θ = 17–19° and 31–32°, which could be unambiguously assigned to LiAlCl$_4$ based on its reported diffraction pattern (Fig. 2).[32,33] In addition to these two phases, a small concentration of incipient LiCl phase is also seen in the sample 250H$_2$-10m. Upon milling for an additional 10 min (sample 250H$_2$-20m), the intensities of Bragg peaks corresponding to LiAlH$_4$ and the LiAlCl$_4$ intermediate are reduced, while those corresponding to

LiCl are enhanced. Only minor amounts of $LiAlH_4$ and $LiAlCl_4$ remain in sample $250H_2$-30m. The formation of AlH_3 could not be discerned in samples $250H_2$-10m and $250H_2$-20m because of the overlap of its Bragg peaks with those from $LiAlH_4$ and $LiAlCl_4$ in the 2θ region between 27–28°; however, the presence of AlH_3 is clearly evident in sample $250H_2$-30m.


Figure 2. X-ray diffraction patterns of the starting mixture ($3LiAlH_4$:$1AlCl_3$) and the products obtained after milling this mixture for 10, 20, and 30 min. Also included is the calculated pattern for $LiAlCl_4$ for comparison. All reactions were carried out at 250 bar H_2 pressure. (*) α-AlH_3, (#) LiCl, and (°) $LiAlH_4$. (inset) Expanded 2θ region between 20–40°. The as-received $AlCl_3$ is strongly textured, but the texturing is greatly reduced after ball milling. Therefore, the intensities of Bragg peaks corresponding to $AlCl_3$ in the physical mixture of $3LiAlH_4$:$1AlCl_3$ are not representative. The X-ray diffraction pattern of ball-milled (un-textured) $AlCl_3$ is shown in Fig. 5.

The sequence of events during the mechanochemical process was also monitored by SSNMR spectroscopy. The ^{27}Al DPMAS and ^{27}Al{^{1}H} CPMAS spectra of the starting mixture and the ball-milled products are shown in Fig. 3a and b. The DPMAS spectrum shows that $AlCl_3$ is almost entirely consumed within the first 10 min of milling. The resonance bands centered around 100 ppm and 15 ppm represent the resulting four- (Al^{IV}) and six-coordinated Al (Al^{VI}) species, respectively. The Al^{VI} signal consists of several superimposed resonances, all of which originate from protonated species as evidenced by the CPMAS spectrum. We discuss the spectral details based on 2D ^{27}Al 3QMAS experiments in the following section. With the increase of milling time to 20 min ($250H_2$-20m) and 30 min ($250H_2$-30m), the Al^{IV} signal becomes narrower and less intense. Concurrently, the center of gravity of the Al^{VI} signal shifts toward lower frequency. After 60 min of milling ($250H_2$-60m), the Al^{IV} signal is no longer observed, while the Al^{VI} resonance is dominated by a single protonated species.

In samples $250H_2$-10m and $250H_2$-20m, the Al^{IV} signal is assigned to a superposition of the central transition powder patterns from $LiAlH_4$ and $LiAlCl_4$, which overlap too strongly to be resolved in a DPMAS spectrum at 14.1 T. This assignment has been elucidated in our earlier study, based on the DPMAS, CPMAS and MQMAS spectra of $LiAlH_4$ and $LiAlCl_4$ in neat form.[22] The ^{27}Al{^{1}H} CPMAS spectra of samples $250H_2$-10m and $250H_2$-20m (Fig. 3b, traces 2 and 3 from the top) represent the proton-containing component of the Al^{IV} signal ($LiAlH_4$). The evolution of the Al^{VI} line shape may be attributed to the ensuing phase conversion of intermediates such as $HAlCl_2$ and H_2AlCl (presumably also containing six-coordinated aluminum) into AlH_3 or phase transition of different polymorphs of AlH_3 during extended milling.[18,31,34] The 3QMAS spectrum of

$250H_2$-10m (Fig. 4a) confirms the presence of at least three species in the Al^{VI} region, centered at 31, 17 and 8 ppm. We are unable to find any crystal structure report or NMR data for these hydrogen-substituted aluminum halides. Note that in sample $250H_2$-60m the line shape of Al^{VI} is slightly different in the DPMAS and CPMAS spectra, which suggests that even the final product may still contain more than one Al species. Similarly, the horizontal projection of the 3QMAS spectrum of $250H_2$-60m differs from the DPMAS spectrum (Fig. 4c) indicating that the Al^{VI} signal consists of at least two species having different efficiencies of multi-quantum conversion.[35] Further study is needed to fully identify the origin of these two signals.
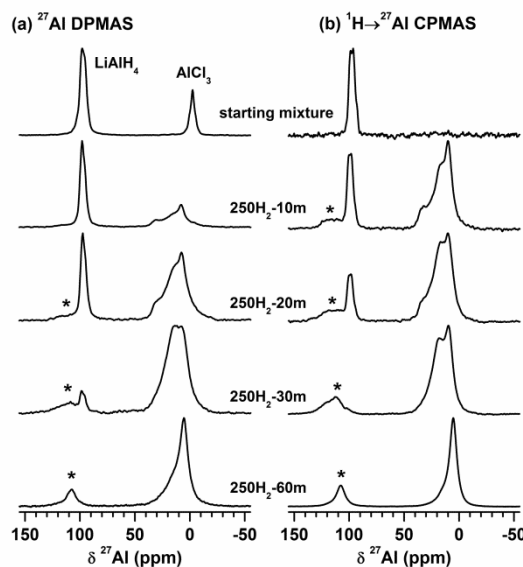
Figure 3. (a) ^{27}Al DPMAS and (b) ^{27}Al{^{1}H} CPMAS spectra of the $3LiAlH_4$+$1AlCl_3$ mixture ball-milled for various times measured at B_0 = 14.1 T. The spectra were normalized to a constant height. The DPMAS spectra were obtained using ν_{RF}^{Al} = 125 kHz, ν_{RF}^{H} = 64 kHz during TPPM ^{1}H decoupling, and τ_{RD} = 1 s. The CPMAS spectra were obtained using ν_{RF}^{Al} = 48 kHz, ν_{RF}^{H} = 64 kHz during cross-polarization and TPPM ^{1}H decoupling, and τ_{RD} = 10 s. The asterisks denote the MAS sidebands.
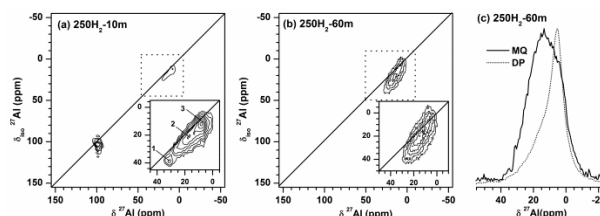
Figure 4. (a) 3QMAS spectrum of $250H_2$-10m, (b) 3QMAS spectrum of $250H_2$-60m, and (c) the horizontal projection of (b). The spectra were obtained at B_0 = 14.1 T using ν_{RF}^{Al} = 125 kHz and 15 kHz for hard and soft (Z-filter) pulses, respectively, and ν_{RF}^{H} = 64 kHz during TPPM ^{1}H decoupling. The data were acquired in 128 rows with Δt_1 = 15.6 μs, and τ_{RD} = 10 s.

These above results might suggest that p_c pertains to the suppression of the decomposition of nascent AlH_3 to metallic Al under the mechanochemical conditions used in these reactions (for example, due to momentary local temperature rise that may become quite large in a high-energy ball mill). This argument, however, is weak since the equilibrium pressure for the reaction shown in Eq. 1

(7,000–25,000 bar) is orders of magnitude higher than pressures used in our experiments (ca. 200 bar). Also, local temperature increases are generally transient (lasting on the order of milliseconds[36]) and the average temperature rise of the entire vial is negligible, compared to the onset of thermal decomposition of AlH_3 (see Fig. 1b). Considering that thermodynamically unstable AlH_3 is kinetically stable at room temperature, millisecond-long temperature spikes should not lead to a measurable decomposition of AlH_3. Furthermore, an uninterrupted milling sequence, in which the vials did not have time to dissipate heat between milling cycles, thereby possibly raising the average temperature in the vials by a few degrees (although the vials were barely warm to the touch immediately after the mill was stopped), does not yield any metallic Al after 60 min of continuous milling at 250 bar. More significantly, we found that milling of the products ($4AlH_3 + 3LiCl$) from the reaction $250H_2$-60m under 1 bar Ar or H_2 pressure does *not* lead to the decomposition of AlH_3 after at least 30 min of milling, suggesting that once formed, AlH_3 remains stable during milling even under very low gas pressures. This observation is, however, in contrast to an earlier report in which pure α-AlH_3 (without LiCl), when milled under 10 bar H_2, completely decomposed to metallic Al in 60 min or less.[37,38] In the following, we analyze in detail the effect of milling conditions (milling intensity/dose rate, gas type and pressure) on the reaction pathway involved in the mechanochemical reaction between $LiAlH_4$ and $AlCl_3$.

Mechanistic Pathway. Although mechanistic aspects of the Schlesinger reaction (Eq. 2) in the solid state have not previously been studied, some insight into the reaction mechanism in Et_2O solution are available in the literature.[37,38] Ashby and Prather[37] studied the reaction between $LiAlH_4$ and $AlCl_3$ in Et_2O at halide-rich compositions of 1:3 and 1:1. Such composition are commonly referred to as "mixed hydride" reagents, and used as reducing agents in both organic and inorganic synthesis. Using infrared spectroscopy and elemental analysis, the products isolated from these reaction mixtures were identified as either $HAlCl_2$ or H_2AlCl, depending on the starting $LiAlH_4$/$AlCl_3$ ratio. It was thus concluded that reduction of $AlCl_3$ by $LiAlH_4$ to AlH_3 proceeds *via* these intermediates. Based on the combined evidence from the PXRD and SSNMR spectroscopy in the present study, some parallels can be drawn between the solution-based processes described above and the solvent-free mechanochemical pathway. Although we believe that this is a dynamic reaction system in which the reactants and the intermediates are continually transformed into the products, the reaction at $p > p_c$ may still be delineated into two broadly defined steps. In the first step, some of the $LiAlH_4$ reacts with all of $AlCl_3$ to form a mixture of $LiAlCl_4$, hydrogen-substituted aluminum chlorides, and/or aluminum trihydride according to the following reaction:

$$xLiAlH_4 + AlCl_3 \rightarrow xLiAlCl_4 + AlCl_{3-4y}H_{4y}, \qquad (4a)$$
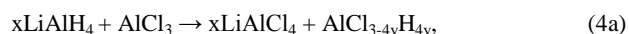
in which, y can be ¼ ($HAlCl_2$), ½ H_2AlCl or ¾ (AlH_3) in a weighted proportion such that the total values of Al, Cl and H are 1, 3-4x and 4x, respectively. In the second step, the so-formed $LiAlCl_4$ and mixture of $AlCl_{3-4y}H_{4y}$ react with the remaining $LiAlH_4$:

$$xLiAlCl_4 + AlCl_{3-4y}H_{4y} + 3-xLiAlH_4 \rightarrow 4AlH_3 + 3LiCl, \qquad (4b)$$

yielding the overall reaction shown in Eq. 3.

To elucidate the dependence of the reaction course on the applied pressure, we examined reactions 4*a* and 4*b* separately in two different experiments. In the first experiment, $LiAlH_4$ and $AlCl_3$ were processed in the molar ratio of ¾:1 (for x= ¾) in a high-energy SPEX mill under ambient argon pressure. The value of x was chosen according to the following model reaction:

$$3/4LiAlH_4 + AlCl_3 \rightarrow 3/4LiAlCl_4 + AlH_3 \qquad (5a)$$

After 1 h of milling, the PXRD pattern (Fig. 5*g*) indicates the formation of the $LiAlCl_4$ phase without the presence of any detectable amounts of metallic Al. It thus becomes clear that pressure dependence of this mechanochemical reaction pathway is not linked to the first step (reaction 4*a*), but to the second step (reaction 4*b*), as confirmed below. It also implies that reaction 4*a* is a common pathway irrespective of the applied pressure regimes, which in turn explains the formation of a small amount of aluminum hydride even below p_c, as observed by the release of hydrogen from the sample $100H_2$-30m. A quantitative analysis of the DPMAS spectrum (ESI, Fig. S1, spectrum *d*, left panel), recorded for the ¾$LiAlH_4$:1$AlCl_3$ mixture after the mechanochemical reaction is complete, reveals the presence of Al^{IV} (originating from $LiAlCl_4$, as substantiated by the $^{27}Al\{^1H\}$ CPMAS spectra (right panel) and the PXRD data shown in Fig. 5*g*) and Al^{VI} species (characteristically broad signal centered at 15 ppm) in the ratio of ca. 0.6:1, which is close to the expected ratio of 0.75:1 for reaction 5*a*. Thereafter, several reactions with the composition $xLiAlH_4$:1$AlCl_3$ were performed under near-ambient argon pressure with x varying from 0.1 to 1.25. The PXRD patterns of the resulting products are shown in Fig. 5*d*–*h*, along with the corresponding patterns for $LiAlCl_4$ (calculated) and milled $AlCl_3$. Although at x = 0.1 the formation of $LiAlCl_4$ is difficult to detect due to low concentration, for x = 0.25 the $LiAlCl_4$ phase is present in equilibrium with the remaining excess $AlCl_3$ (considering the stoichiometry of reaction 5*a*). No new or unidentified Bragg reflections that may arise from the hydrogen-substituted aluminum chlorides or AlH_3 phases were observed, suggesting that these phases are present in the amorphous form. At x=0.75, only the $LiAlCl_4$-type phase could be detected, indicating that the reaction is stoichiometric. The ^{27}Al SSNMR data were collected for samples with fractional compositions (x = 0.25, 033 and 0.5) in order to be able to identify and distinguish species such as H_2AlCl and $HAlCl_2$, but the signals, while clearly suggesting the presence of multiple species, could not be unambiguously deconvoluted (ESI, Fig. S2)
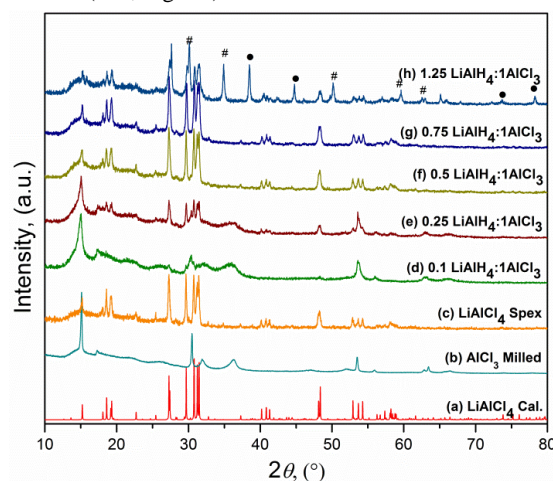
Figure 5. X-ray diffraction patterns of products obtained from milling of $xLiAlH_4$:1$AlCl_3$ mixtures (x=0.1–1.25) in SPEX mill under near-ambient argon pressure for 60 min. (#) LiCl, (●) metallic Al.

For x=1.25, metallic Al is clearly detected together with LiCl which is in concurrence with the suggested reaction of the intermediates $LiAlCl_4$ and $AlCl_{3-4y}H_{4y}$ with excess $LiAlH_4$ according to reaction 4*b*; however, because it occurs below p_c, it leads to the formation of metallic Al (pattern *h*). Pressure build-up in the vessel after the completion of the reaction was accordingly observed for x = 1.25, but not for the other examined stoichiometries.

The TPD of the product from the x=0.75 reaction (not shown) is typical of the thermal decomposition of AlH_3; the total yield of 1.8 wt % hydrogen is in good agreement with the expected theoretical capacity of 1.85 wt%, suggesting that i) the reaction 5a is quantitative, and ii) all of the hydrogen is retained in the system, and is associated with Al^{VI} after the milling.

Reaction 4b in the proposed pathway, and the dependence of its final products on applied pressure, was also confirmed independently of the first step *via* two different approaches.

Approach 1: In the first case, the product obtained from reaction 5a ($3/4LiAlH_4:1AlCl_3$ in SPEX mill) was mixed with additional 9/4 mole eq. of $LiAlH_4$, i.e. by adding $LiAlH_4$ in a stoichiometric amount corresponding to a $3LiAlH_4:1AlCl_3$ overall reaction. This mixture was then processed in a Fritsch mill under hydrogen pressure using the *standard milling conditions*. As expected, the reaction carried out at 250 bar H_2 yields only α-AlH_3 and LiCl, whereas the reaction at 100 bar H_2 predominantly yields metallic Al and LiCl as shown below in Eqs. 5b and 5c respectively (assuming 60/40 overall conversion into Al/AlH_3; see above and Ref. 13), and in Fig. 6a.

$$\frac{3}{4}\,LiAlH_4 + AlCl_3 \xrightarrow{\text{SPEX, Ar}} \frac{3}{4}\,LiAlCl_4 + AlH_3 \dots\dots\dots\dots\dots\dots\dots(5a)$$

$$\left.\frac{3}{4}\,LiAlCl_4 + AlH_3 + \frac{9}{4}\,LiAlH_4\right\} \begin{array}{l} \xrightarrow{\text{250 b } H_2} 4AlH_3 + 3LiCl\dots\dots\dots\dots\dots(5b) \\ \xrightarrow{\text{100 b } H_2} 2.4Al + 1.6AlH_3 + 3LiCl + 3.6H_2\dots(5c) \end{array}$$

Approach 1
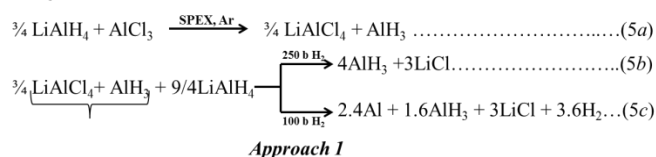
As discussed above, once formed, AlH_3 is stable during the mechanochemical processing. Therefore, the mechanochemical reaction between 1 mole eq. of $LiAlCl_4$ and 3 mole eq. of $LiAlH_4$ at pressures below p_c leads to the conversion of 0.8 mole eq. of Al to AlH_3, while the remaining 3.2 mole eq. of Al available in both $LiAlCl_4$ and $LiAlH_4$ is converted into metallic Al. Appearance of small amounts of both α-AlH_3 and α'-AlH_3 phases in the reaction completed at 100 bar H_2 is in line with the products obtained from the 3:1 $LiAlH_4:AlCl_3$ reactions carried out at $p < p_c$ (Fig. 6a, pattern 5b). Desorption characteristics of the sample prepared by utilizing reaction 5a followed by processing at 250 bar (reaction 5b) is typical of pure AlH_3 yielding 4.8 wt % H_2, which is in excellent agreement with the net reaction 3 with nearly quantitative yield.

Approach 2: In this approach, pure $LiAlCl_4$ was first prepared by reacting 1:1 molar mixture of LiCl and $AlCl_3$ in a SPEX mill (reaction 6a). After 60 min of milling, X-ray pure $LiAlCl_4$ was obtained (Fig. 6b, pattern 6a), which was then milled with $LiAlH_4$ in a Fritsch mill under *standard milling conditions* at 250 bar H_2 (reaction 6b) and 100 bar H_2 (reaction 6c) with an overall composition of 1:3 (reaction 6c below is written assuming the same rate of conversion of the four-coordinated aluminum into metallic Al and AlH_3 as reaction 5c).

$$LiCl + AlCl_3 \xrightarrow{\text{SPEX, Ar}} LiAlCl_4 \dots\dots\dots\dots\dots\dots\dots\dots(6a)$$

$$\left. LiAlCl_4 + 3LiAlH_4\right\} \begin{array}{l} \xrightarrow{\text{250 b } H_2} 4AlH_3 + 4LiCl\dots\dots\dots\dots\dots(6b) \\ \xrightarrow{\text{100 b } H_2} 3.2Al + 0.8AlH_3 + 4LiCl + 4.8H_2\dots(6c) \end{array}$$
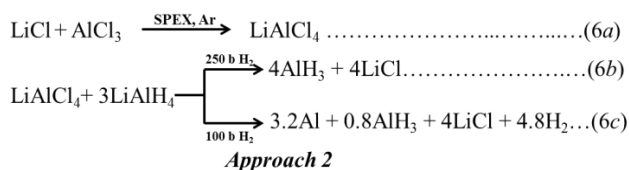
Approach 2

Fig. 6b also shows the PXRD patterns of samples prepared by the two reactions carried out above and below p_c. As expected, the reaction at 250 bar yields α-AlH_3 and LiCl, whereas the reaction at 100 bar yields metallic Al and LiCl, and only a minor fraction of mixture of α-AlH_3 and α'-AlH_3. The relative intensities of Bragg peaks in Fig. 6 are consistent with the higher concentrations of AlH_3 in reactions 5b and 5c, compared to reactions 6b and 6c.
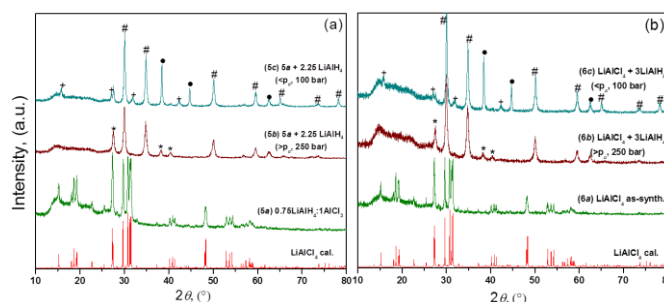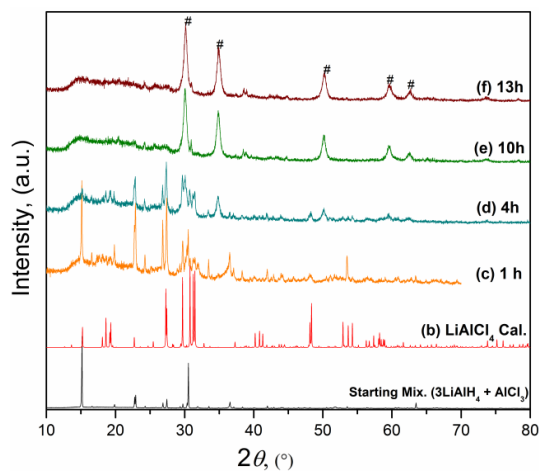

Figure 6. X-ray diffraction patterns of the products obtained a) after milling products obtained from reaction *a* with $LiAlH_4$ with final composition of $3LiAlH_4: 1AlCl_3$ and b) after milling the pre-formed $LiAlCl_4$ with $LiAlH_4$ (final composition 3:1 according to reaction *c* carried out above and below the critical pressure. (*) α-AlH_3, (#) LiCl, (●) metallic Al, (+) α'-AlH_3.

Effect of milling intensity on p_c. To examine whether or not p_c is related to the milling parameters and therefore to the milling intensity, the rotation speed was reduced from 300 to 150 rpm, while keeping b:p (~160:1) unchanged. As expected, the progress of reactions 4a and 4b was considerably slower due to lower shear and strain rates, and also due to reduced mass transport; it takes between 10–13 h to approach completion, as shown in Fig 7. Quite surprisingly, however, by lowering the rotation speed to 150 rpm, formation of metallic Al can be completely suppressed even at ~1 bar of H_2 pressure. Although the reaction nears completion only after 10 h of milling, the Bragg peaks from the intermediate $LiAlCl_4$ are clearly seen after 60 min along with those from the unreacted $LiAlH_4$. Consistent with the experimental evidence described in the previous section, this suggests that reaction 4a proceeds relatively quickly, followed by a slower reaction 4b. It may also be noted that the longer processing time results in greater disorder or much smaller crystallites of AlH_3, so much so that the latter becomes X-ray amorphous, and it becomes much more difficult to detect in PXRD patterns with Cu $K_{\alpha 1}$ radiation. Nevertheless, the absence of metallic Al, the desorption behavior of the sample obtained after 13 h (ESI, Fig S3.), and the SSNMR spectra (ESI, Fig S1 spectrum *e*.) are all in good agreement with the nearly quantitative formation of AlH_3 according to the overall reaction 3. Reduction in the formation of metallic Al at room temperature was also noted by Paskevicius *et al*. when the milling intensity was lowered by reducing both the ball size and b:p ratio.[18] As in the present case, the authors also noted a loss in crystallinity of AlH_3 upon extended milling for up to 6 h. However, in contrast to our results, in this previous work hydrogen desorption measurements indicated that ~66 % of the total Al was converted into metallic Al after 6 h of milling at room temperature.

To test the possibility of reducing the reaction time at 1 bar H_2, the milling speed was ramped to 180 and 230 rpm. Both of these attempts failed, however, resulting in the formation of metallic Al. Although metallic Al was not formed at 170 rpm, only a minor increase in the reaction rate (the reaction was near completion in 12 h) was observed as compared with the reaction at 150 rpm.

Effect of gas type. We also elucidated the role of gas pressure in directing the reaction pathway in a given milling regime (i.e keeping the milling parameters constant). In an experiment designed for this purpose, products obtained from the mechanochemical reaction between $LiAlD_4$ and $AlCl_3$ in H_2 were analyzed by SSNMR. Figure 8 shows the ^{27}Al DP and $^{27}Al\{^1H\}$ CPMAS spectra of $3LiAlD_4:1AlCl_3$ (milled under 250 bar H_2 for 60 min). The DPMAS spectrum was similar to the one observed for $3LiAlH_4:1AlCl_3$ ($250H_2$-60m), whereas the $\{^1H\}$-CPMAS signal practically

disappears, which suggests that no gas-solid exchange occurs during the reaction. This result confirms that gaseous hydrogen is not chemically involved in the reaction as one may expect, given the stoichiometric nature of the reaction in either the ether solution [12–14] or in this work. This finding, however, further implies that the reaction may as well be carried out in other inert gases such as He or Ar.

Figure 7. X-ray diffraction patterns of the products obtained by milling $3LiAlH_4:1AlCl_3$ at 150 rpm (b:p~160:1) under 1 bar H_2 after time intervals as indicated. (#) denotes Bragg peak positions LiCl.

It was also established that the lowest milling speed at which the reaction under pressure (above p_c) could be completed within 1 h was ca. 230 rpm. However, the p_c at this milling speed was not found to be significantly different from that at 300 rpm, namely between 180–210 bar. (ESI, Fig S4.) This indicates that there is a cut-off speed/rate above which the application of pressure becomes essential. Based on these experiments, we conclude that i) there is a threshold mechanical energy delivery rate (controlled by rpm at constant b/p) that requires introduction of gas pressures exceeding p_c in order to suppress reactions 5b and 6c, and ii) once the threshold is reached and exceeded, the reaction kinetics is not changed since all of the reactions are finished within 1 h, and is invariant of the applied pressure.
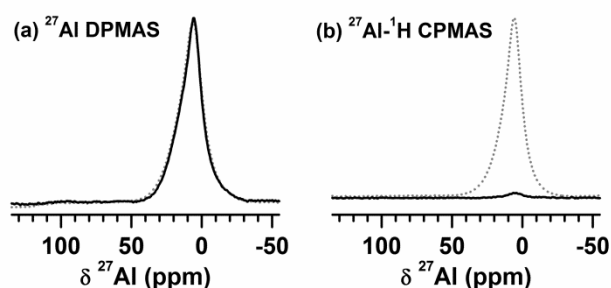
Figure 8. (a) ^{27}Al DP and (b) $^{27}Al-^1H$ CPMAS spectra of $3LiAlD_4:1AlCl_3(250H_2-60m)$. The dotted lines represent the corresponding spectra of $3LiAlH_4:1AlCl_3(250H_2-60m)$. The spectra show absolute height. $B_0 = 9.4$ T. (A) The DPMAS spectra were obtained using $\nu_{RF}^{Al} = 125$ kHz, $\nu_{RF}^H = 64$ kHz for TPPM ^1H decoupling, and $\tau_{RD} = 1$ s. (B) The CPMAS spectra were obtained using $\nu_{RF}^{Al} = 48$ kHz, $\nu_{RF}^H = 64$ kHz for cross-polarization and TPPM ^1H decoupling, and $\tau_{RD} = 10$ s.

We therefore examined this mechanochemical reaction under He and Ar pressures. The PXRD patterns of products milled under P^{He} and P_{Ar} are shown in Fig. 9 patterns *b* and *c*, and patterns *d, e* and *f*, respectively. Under *standard milling conditions*, in contrast to the

reactions under H_2, metallic Al was detected only in the samples that were milled under $P_{He} \leq 125$ bar and $P_{Ar} < 90$ bar. Thus, in general p_c drops when a gas with higher molecular weight is used, which demonstrates that p_c is affected by the physical properties of the ambient atmosphere, i.e. by the simple presence of *high-pressure gas as a processing medium*. Although p_c is lowered in a He atmosphere when compared to H_2, the reaction is still complete within 60 min (150He-60m). This serves as evidence that the drop in p_c is not necessarily a manifestation of a lower reaction rate but is rather controlled by the mechanical energy dose rate. In Ar, reaction kinetics is slower as noted by the presence of unreacted $LiAlH_4$ after 60 min (90Ar-60m), perhaps due to a more severe obstruction of the motion of the balls by the denser gaseous medium. Further details of reactions under argon pressure are given as supplementary information in Fig. S5.
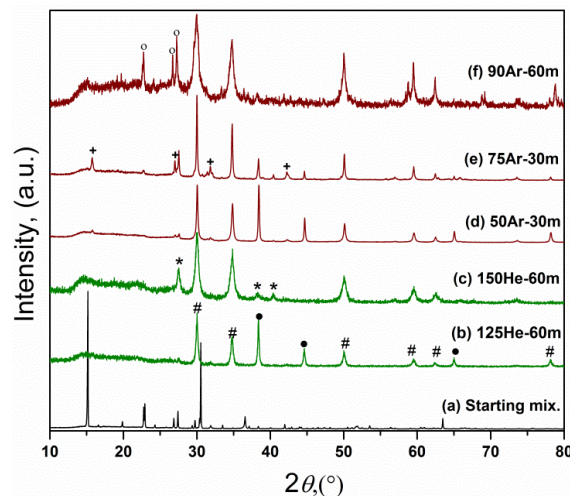
Figure 9. X-ray diffraction patterns of products from $3LiAlH_4:1AlCl_3$ milled under various He and Ar pressure. (*) α - AlH_3, (#) LiCl, (●) metallic Al, (+) α'-AlH₃, and (°) $LiAlH_4$

Existence of p_c. The results described above clearly highlight several novel aspects of the mechanochemical processing under gas pressure. Although the mechanically activated reactions of solids with reactive gases are well known in mechanochemistry,[19] the potential of purely physical control of reaction pathways by gas pressure has not been noted earlier. Since it is established in this work that gaseous hydrogen is non-reactive during the progress of 3:1 $LiAlH_4:AlCl_3$ reaction, and it can be effectively substituted by He or Ar, it is clear that the origin of the critical pressure lies in the physical properties of employed gases, such as their density, viscosity, and heat capacity. All things considered, we believe that gas under high pressure acts like a fluid medium (akin to liquid-assisted milling) which effectively controls the mechanical energy dose rate along with the usual milling parameters that define milling energies (e.g. rpm, b/p, size and density of the balls, and type of mill). Hence, the following four postulates may provide a reasonable explanation for the existence of p_c: i) the specific heat of a gas increases with increasing pressure, which therefore provides faster and more effective removal of heat generated during the milling; (ii) the viscosity of a gas increases with increasing pressure, leading to a proportional reduction of the kinetic energy of the balls, thus lowering the mechanical energy dose rate delivered to the reactants, intermediates and products; (iii) since the starting materials, intermediates, and products are soft, their compressibilities are high, and therefore, diffusivity of ions should be strongly affected by the increasing pressure, in turn affecting the reaction pathway(s); and (iv) any change in the applied pressure may alter the microstructural evolution and hence change the reaction pathway(s), which partly

explains why other systems (e.g. $3NaAlH_4$-$AlCl_3$) show much different p_c values when processed under identical conditions.[39]

Experimental evidence also suggests that metallic Al that forms at p $< p_c$ is not likely to result from the decomposition of nascent AlH_3 due to heat generated during milling (see reaction 4a and relevant discussion). Although milling under cryogenic temperature suppresses the formation of metallic Al,[17] it is unclear whether prevention of AlH_3 decomposition or an effect similar to that caused by the elevated gaseous medium pressure, i.e. effective reduction of the mechanical energy dose rate, is responsible. It is worth mentioning here that the piston-driven SPEX-freezer mill used for cryomilling in Ref. 17 is a relatively low-energy mill.

Towards identifying the atomistic mechanism. Although the mechanochemical pathway of this reaction is unequivocally established by the results described above, the actual atomistic mechanism of any and all of the reactions 4a – 6c remains elusive. What appears to be clear is that initially at least a part of the six-coordinated aluminum in $AlCl_3$ is converted into the four-coordinated aluminum in $LiAlCl_4$, which is followed by its retransformation into the six-coordinated aluminum in alane. Although the formation of $LiAlCl_4$, which has not been identified as an intermediate in the Schlesinger reaction, is established beyond doubt, its actual role during the reaction remains unclear. In a most likely scenario, the multiple signals from Al^{IV} and Al^{VI} species (all of which are hydrogenated after 10 min, see Fig. 3) may result from replacing Cl in $LiAlCl_4$ ($AlCl_3$) with hydrogen or vice versa in $LiAlH_4$ (AlH_3), leading to formation of $LiAlCl_{4-x}H_x$ (x = 1, 2, 3) and/or $AlCl_{3-x}H_x$ (x = 1, 2) species.[37] The former have not been reported nor identified in the past. The latter, which have been isolated in pure form [37] or as coordination complexes,[38] are known to exist but their crystal or molecular structures have not been reported. Further, it is likely that $LiAlCl_{4-x}H_x$ intermediate species are highly unstable; therefore, their identification outside the ball milling vial may be impossible. Yet, considering that all of the Al atoms in the final product are coordinated by six hydrogen atoms, formation of such species, which are likely short lived, seems inevitable. Regardless of difficulties with experimental identification and characterization of these and perhaps other highly transient species, recent advancements in density functional theory may prove useful in estimating their structures, stability and energetics. Such efforts are underway, and their results will be reported when they become available.

Conclusions

A quick and an efficient mechanochemical method for synthesis of AlH_3 from a $3LiAlH_4$:$1AlCl_3$ mixture at room temperature has been developed, and the reaction pathway has been studied. With the application of moderate pressures of various gases (H_2, He or Ar), side reactions that lead to the formation of metallic Al are entirely suppressed, and a nearly complete conversion of all available Al into AlH_3 is achieved between 30–60 minutes. The ability to successfully synthesize alane via mechanochemistry at room temperature eliminates the need for large amounts of solvents or cryogenic cooling to suppress the formation of metallic Al. It is determined that $LiAlCl_4$ is formed as an intermediate during the first step of the reaction, which then reacts further with $LiAlH_4$ to form alane and LiCl. We also demonstrated for the first time that control of mechanical energy dose rate is critical for controlling the reaction pathway, and that it could be influenced by the applied gas pressure during processing. Moreover, the soft nature of the precursors leads to a very clean milling process with minimal contamination from the milling tools. Although the dry mechanochemical process proposed here for the synthesis of AlH_3 results in a non-solvated product,

obtaining pure AlH_3 would of course require removal of the lithium chloride byproduct.

Notes and references

[a] Ames Laboratory, Iowa State University, Ames, IA 500011-3020, USA. E-mail address: shalabh@ameslab.gov, vitkp@ameslab.gov, mpruski@ameslab.gov.

[b] Department of Chemistry, Iowa State University, Ames, IA 500011-3111, USA

[c] Department of Materials Science and Engineering, Iowa State University, Ames, IA 50011-2300, USA

Electronic Supplementary Information (ESI) available: XRD patterns and SSNMR spectra of samples made with fractional compositions, SSNMR and TPD of the sample prepared at 150 rpm, and time dependent XRD analysis of products formed at 230 rpm. See DOI: 10.1039/b000000x/

1   J.O. Keller, L.E. Klebanoff, S. Schoenung, M. Gillie, in *Hydrogen Storage Technology: Materials and Applications* (Ed: L.E. Klebanoff.), Taylor and Francis, Boca Raton, USA, 2012, Ch. 1

2   Alternative Fuels Data Center, U.S. Department of Energy, Energy Efficiency & Renewable Energy, http://www.afdc.energy.gov/fuels/hydrogen_basics.html, accessed: April, 2014.

3   L. Schlapbach, A. Züttel, *Nature* 2001, *414*, 353.

4   U. Eberle, M. Felderhoff, F. Schüth, *Angew. Chem. Int. Ed.*, 2009, *48*, 6608.

5   O. Bičáková, P. Straka, *Int. J. Hydrogen Energy*, 2012, *37*, 11563.

6   D. A. Anton, T. Motyka, T. *US DOE Hydrogen Program Annual Merit Review Proceedings*, Arlington (VA); http://www.hydrogen.energy.gov/pdfs/review12/st004_anton_2012_o.pdf, accessed: April, 2014; J. M. Pasini, C. Corgnale, B. A. van Hassel, T. Motyka, S. Kumar, K. L. Simmons, *Int. J. Hydrogen Energy*, 2013, *38*, 9755.

7   J. Graetz, J. J. Reilly, V. A. Yartys, J. P. Maehlen, B. M. Bulychev, V. E. Antonov, B. P. Tarasov, I. E. Gabis, *J. Alloys Compd.*, 2011, *509*, S517.

8   R.K. Ahluwalia, T.Q. Hua, J.K. Peng, *Int. J. Hydrogen Energy*, 2012, *37*, 2891.

9   C.L. Aardahl, S.D. Rassat, *Int. J. Hydrogen Energy*, 2009, *34*, 6676.

10 G. C. Sinke, L. C. Walker, F. L. Oetting, D. R. Stull, *J. Chem. Phys.*, 1967, *47*, 2759; J. Graetz, J. Reilly, *J. Alloys Compd.*, 2006, *424*, 262.

11 S. K. Konovalov, B. M. Bulychev, *Inorg. Chem.*,1995, *34*, 172; J. Graetz, S. Chaudhuri, Y. Lee, T. Vogt, J. J. Reilly, *Phys. Rev. B* 2006, *74*, 214114.

12 A. E. Finholt, A. C. Bond Jr., H. I. Schlesinger, *J. Am. Chem. Soc.*, 1947, *69*, 1199.

13 G. Chizinsky, G. G. Evans, T. R. P. Gibb Jr., M. J. Rice Jr., *J. Am. Chem. Soc.*, 1955, *77*, 3164.

14 D. L. Schmidt, R. W. Diesen, (Dow Chemical Co.) *U.S.* Patent 3 840 654, 1974; N. E. Matzek, D. F. Musinski, (Dow Chemical Co.) *U.S.* Patent 3 819 819, 1974; F. M. Brower, N. E. Matzek, P.

F. Reigler, H. W. Rinn, C. B. Roberts, D. L. Schmidt, J. A. Snover, K. Terada, *J. Am. Chem. Soc*., 1976, *98*, 2450.

15 L. V. Dinh, D. A. Knight, M. Paskevicius, C. E. Buckley, R. Zidan, *Appl. Phys. A*, 2012, *107*, 173.

16 S. Gupta, I. Hlova, V. K. Pecharsky, Unpublished.

17 H. W. Brinks, A. Istad-Lem, B. C. Hauback, *J. Phys. Chem. B*, 2006, *110*, 25833.

18 M. Paskevicius, D. A. Sheppard, C. E. Buckley, *J. Alloys and Compd.*, 2009, *487*, 370.

19 J. Huot, D. B. Ravnsbæk, J. Zhang, F. Cuevas, M. Latroche, T. R. Jensen, *Prog. Mater. Sci.*, 2013, *58*, 28.

20 O. Friedrichs, A. Borgschulte, S. Kato, F. Buchter, R. Gremaud, A. Remhof, A. Züttel, *Chem. Eur. J.*, 2009, *15*, 5531.

21 H. Shao, M. Felderhoff, F. Schüth, *Int. J. Hydrogen Energy*, 2011, *36*, 10828.

22 I. Z. Hlova, S. Gupta, J. F. Goldston, T. Kobayashi, M. Pruski, V. K. Pecharsky, *Faraday Discuss*., 2014, DOI: 10.1039/C3FD00161J.

23 J. W. Wiench, V. P. Balema, V. K. Pecharsky, M. Pruski, *J. Solid State Chem.*, 2004, *177*, 648.

24 D. Freude, J. Haase, *NMR Basic Principles Progr.*, 1993, *29*, 1.

25 A. E. Bennett, C. M. Rienstra, V. K. Lakshmi, R. G. Griffin, *J. Chem. Phys.*, 1995, *103*, 6951.

26 L. Frydman, J. S. Harwood, *J. Am. Chem. Soc.*, 1995, *117*, 5367.

27 J. -P. Amoureux, C. Fernandez, S. Steuernageel, *J. Magn. Reson.* 1996, *A123*, 116.

28 J. Turley, H. W. Rinn, *Inorg. Chem*., 1969, *8*, 18.

29 G. Sandrock, J. Reilly, J. Graetz, W. –M. Zhou, J. Johnson, J. Wegrzyn, *Appl. Phys. A*, 2005, *80*, 687.

30 J. Graetz, J. Reilly, *J. Phys. Chem. B*, 2005, *109*, 22181.

31 S. Orimo, Y. Nakamori, T. Kato, C. Brown, C. M. Jensen, *Appl. Phys. A*, 2006, *83*, 5.

32 International Center for Diffraction Data, PDF-23-35; $LiAlCl_4$ crystallizes with a monoclinic structure in the $P2_1/c$ space group. The structure features distorted $AlCl_4$ tetrahedra and $LiCl_6$ octahedra. The structure of $LiAlCl_4$ is closely related to that of $LiAlH_4$, which also crystallizes in the same space group and consists of AlH_4 tetrahedra. In contrast to the six coordinated lithium atom in $LiAlCl_4$ however, the lithium atoms in $LiAlH_4$ is surrounded by five hydrogen atoms to form trigonal bipyramidal coordination.

33 G. Mairesse, P. Barbier, J. P. Wignacourt, P. Baert, *Cryst. Struct. Commun.*, 1977, *6*, 15.

34 S. –J. Hwang, R. C. Bowman Jr., J. Graetz, J. J. Reilly, W. Langley, C. M. Jensen, *J. Alloys and Compd.*, 2007, *446–447*, 290.

35 M. Pruski, A. Bailly, D. P. Lang, J. P. Amoureux, C. Fernandez, *Chem. Phys. Lett.*, 1999, *307*, 35.

36 R. B. Schwarz, C. C. Koch, C. C. *Appl. Phys. Lett.*, 1986, *49*, 146.

37 E. C. Ashby, J. Prather, *J. Amer. Chem. Soc.*, 1966, *88*, 729.

38 E. Wiberg, K. Mödritzer, R. U. Lacal, *Rev. Acad. Cienc. Exactas, Fis, Quim. Nat.*, 1954, *9*, 91.

39 S. Gupta, I. Z. Hlova, J. F. Goldston, T. Kobayashi, M. Pruski, V. K. Pecharsky, unpublished.

Green Chemistry Accepted Manuscript